OPEN ACCESS
IOP Publishing

Journal of Physics D: Applied Physics

J. Phys. D: Appl. Phys. 55 (2022) 404006 (9pp)

https://doi.org/10.1088/1361-6463/ac83d3

Theoretical analysis and modelling of degradation for III–V lasers on Si

Jianzhuo Liu[1,2], Mingchu Tang[1,*], Huiwen Deng[1], Samuel Shutts[3], Lingfang Wang[4], Peter M Smowton[3], Chaoyuan Jin[4,5], Siming Chen[1], Alywn Seeds[1] and Huiyun Liu[1]

[1] Department of Electronic and Electrical Engineering, University College London, Torrington Place, London WC1E 7JE, United Kingdom
[2] Changchun Institute of Optics, Fine Mechanics and Physics, Chinese Academy of Sciences, Changchun 130033, People's Republic of China
[3] School of Physics and Astronomy, Cardiff University, Cardiff CF10 3AT, United Kingdom
[4] College of Information Science and Electronic Engineering, Zhejiang University, Hangzhou 310007, People's Republic of China
[5] Zhejiang Lab, Hangzhou 311121, People's Republic of China

E-mail: mingchu.tang.11@ucl.ac.uk

Received 21 April 2022, revised 15 July 2022
Accepted for publication 25 July 2022
Published 4 August 2022

Abstract

InAs/GaAs quantum-dot (QD) lasers offer a promising method to realise Si-based on-chip light sources. However, the monolithic integration of III–V materials on Si introduces a high density of threading dislocations (TDs), which limits the performance of such a laser device in terms of device lifetime. Here, we proposed a kinetic model including a degradation term and a saturation term to simulate the degradation process caused by the TDs in the early stage of laser operation. By using a rate equation model, the current density in the wetting layer, where the TDs concentrate, is calculated. We compared the rate of degradation of QD lasers with different cavity lengths and of quantum-well lasers, where both are directly grown on Si substrates, by varying the fitting parameters in the calculation of current densities in the kinetic model.

Keywords: quantum dot lasers, quantum well lasers, semiconductor defects, semiconductor laser modelling

(Some figures may appear in colour only in the online journal)

1. Introduction

The dramatically increasing demands of data traffic such as 5G infrastructures urge the development of high-speed and low-cost data transmission [1, 2]. Photonic integrated circuits (PICs) based on the Si platform have gained significant attention due to their advantages in low cost and high bandwidth data-transmission [3, 4]. In the field of photon-based quantum computing techniques, a fully photon operated device will play a key role and significantly accelerate its development and optimization [5]. The efficient electrically pumped Si-based light-emitting sources is a necessary for the commercialization of Si-based PICs [6]. As active components in PICs, the optical and electrical properties of group III–V materials are superior to group IV materials. Heterogeneous, monolithic and transfer printing are main ways to integrate III–V materials on Si substrates [7, 8]. The direct growth of III–V materials on the Si platform has been regarded as one of the most promising techniques for on-chip light sources [9, 10]. However, the high threading dislocation density (TDD) caused by the large lattice mismatch and the difference in the thermal expansion coefficient between III–V compound semiconductors and Si substrate gives rise to the

[*] Author to whom any correspondence should be addressed.

Original content from this work may be used under the terms of the Creative Commons Attribution 4.0 licence. Any further distribution of this work must maintain attribution to the author(s) and the title of the work, journal citation and DOI.

formation of non-radiative recombination centres [11–14]. These defects and accompanying recombination enhanced defect reactions (REDR) dramatically reduce the quality of III–V materials and increase the junction temperature thus degrading the operating performance and lifetime of devices fabricated from them [15–17]. To improve the thermal stability of devices, the efficient heat dissipation has been employed, such as metallic substrates, heat sink [18–20]. The higher the dislocation density that is present, the more rapid is the rate of degradation.

Quantum-well (QW) and quantum-dot (QD) laser have been assumed an ideal source for Si-based PICs. However, the performance of QW and QD lasers directly grown on Si substrates has significant difference considering the impact of high density of threading dislocations (TDs). For GaAs based QW lasers epitaxially grown on Si, the longest reported lifetime is around 200 h under room temperature testing [21]. For 1.3 μm Si-based InAs/GaAs QD lasers grown on the GaAs/Si virtual substrate, the extrapolated laser lifetime can reach more than 1000 000 h by ageing it at 35 °C under a constant current injection of 1.75 times of initial threshold [16, 22]. The mechanism underlying the higher performance of QD lasers grown on Si is explained through the experimental comparison with QW lasers, where the effect of TDs on the active regions in Si-based lasers is well understood [23, 24]. Here we focus on applying a similar theoretical model to both QW and QD lasers grown on Si.

In theory, when an electron is captured by a deep level (formed due to the defect state) with a subsequent capture of a hole, multi-phonon emission occurs, which results in strong vibration of the defect atoms, and motivates the defect motion such as migration, creation, or clustering [25]. According to the above phenomena, a kinetic model for the QW laser operating under the constant optical power ageing condition was proposed [26]. However, the theory merely matches to the experimental degradation caused by point defects, which does not include effects between point defects.

In this article, we employ a kinetic model and consider the characteristic of TDs that the interaction of TDs strongly affects the degradation, which introduces more TDs during the device operating. The interaction would reduce the rate of degradation because of the energy consumption of the vibration among the defects. This leads to a theoretical model that assumes that the rate of growth of defects abates and eventually saturates, which describes the change of threshold current (I_{th}) as a function of the ageing time and explains the degradation of QD and QW lasers at a more fundamental level. To simplify the model, we assume that the rate of the TD creation does not continue abating, by using a classic population growth model to represent the saturation term. Since the relative number of QDs directly affected by TDs is very low, the carriers in the wetting layer (WL), QW and barrier layer (BL) are the major factor that affects the degradation of QD and QW lasers respectively. The degradation is relatively easy to saturate at early stage, followed by a much lower rate of long-term degradation [27]. Our work mainly focuses on the degradation in the early stage.

2. Theoretical model

The QD structure is based on a 1.3 μm InAs/GaAs QD laser monolithically grown on GaAs/Si virtual substrate, which including GaAs/Si buffer layer and five layers of dot-in-well (DWELL) structure as active region. The DWELL consists of 3ML InAs QDs grown on a 2 nm of $\mathrm{In_{0.15}Ga_{0.85}As}$ layer and capped with 5 nm of $\mathrm{In_{0.15}Ga_{0.85}As}$ layer. In order to examine the carrier densities in QD structures, a multi-level rate equation travelling-wave model with one dimensional spatial resolution along the longitudinal direction of the laser is used to calculate the carrier dynamics [28]. The rate of change of the electron density in BL, WL, second excited state (ES2), first excited state (ES1) and ground state (GS) in a InAs/GaAs QD laser of length L and section w (waveguide width) $\times$ Δz (space step discretizing L) can be expressed as [23]:

$$\frac{dN^e_{\mathrm{BL}}}{dt} = \frac{\eta I}{e}\frac{\Delta z}{L} + \frac{N^e_{\mathrm{WL}} f^{e\prime}_{\mathrm{BL}}}{\tau^{\mathrm{WL},e}_{\mathrm{esc}}} - \frac{N^e_{\mathrm{BL}} f^{e\prime}_{\mathrm{WL}}}{\tau^{\mathrm{WL},e}_{c}} - \frac{N^e_{\mathrm{BL}}}{\tau^{\mathrm{BL}}_{\mathrm{nr}}} - \frac{N^e_{\mathrm{BL}}}{\tau^{\mathrm{BL},e}_{\mathrm{dis}}} \quad (1)$$

$$\frac{dN^e_{\mathrm{WL}}}{dt} = \frac{N^e_{\mathrm{BL}} f^{e\prime}_{\mathrm{WL}}}{\tau^{\mathrm{WL},e}_{c}} + \frac{N^e_{\mathrm{ES2}} f^{e\prime}_{\mathrm{WL}}}{\tau^{\mathrm{ES2},e}_{\mathrm{esc}}} - \frac{N^e_{\mathrm{WL}} f^{e\prime}_{\mathrm{BL}}}{\tau^{\mathrm{WL},e}_{\mathrm{esc}}} - \frac{N^e_{\mathrm{WL}} f^{e\prime}_{\mathrm{ES2}}}{\tau^{\mathrm{QD},e}_{c}} - \frac{N^e_{\mathrm{WL}}}{\tau^{\mathrm{WL}}_{\mathrm{nr}}} - \frac{N^e_{\mathrm{WL}}}{\tau^{\mathrm{WL},e}_{\mathrm{dis}}} \quad (2)$$

$$\frac{dN^e_{\mathrm{ES2}}}{dt} = \frac{N^e_{\mathrm{WL}} f^{e\prime}_{\mathrm{ES2}}}{\tau^{\mathrm{QD},e}_{c}} + \frac{N^e_{\mathrm{ES1}} f^{e\prime}_{\mathrm{ES2}}}{\tau^{\mathrm{ES1},e}_{\mathrm{esc}}} - \frac{N^e_{\mathrm{ES2}} f^{e\prime}_{\mathrm{WL}}}{\tau^{\mathrm{ES2},e}_{\mathrm{esc}}} - \frac{N^e_{\mathrm{ES2}} f^{e\prime}_{\mathrm{ES1}}}{\tau^{e}_{0}} - \frac{N^e_{\mathrm{ES2}}}{\tau^{\mathrm{ES2},e}_{\mathrm{nr}}} \quad (3)$$

$$\frac{dN^e_{\mathrm{ES1}}}{dt} = \frac{N^e_{\mathrm{ES2}} f^{e\prime}_{\mathrm{ES1}}}{\tau^{e}_{0}} + \frac{N^e_{\mathrm{GS}} f^{e\prime}_{\mathrm{ES1}}}{\tau^{\mathrm{GS},e}_{\mathrm{esc}}} - \frac{N^e_{\mathrm{ES1}} f^{e\prime}_{\mathrm{ES2}}}{\tau^{\mathrm{ES1},e}_{\mathrm{esc}}} - \frac{N^e_{\mathrm{ES1}} f^{e\prime}_{\mathrm{GS}}}{\tau^{e}_{0}} - \frac{N^e_{\mathrm{ES1}}}{\tau^{\mathrm{ES1},e}_{\mathrm{nr}}} \quad (4)$$

where $f^{m\prime}_n = (1 - f^m_n)$ is the probability of an empty state in the energy level n; $\eta I/e$ is carrier injection into the BL; $1/\tau_c^{m,e}$, $1/\tau_0^{m,e}$, $1/\tau_{\mathrm{esc}}^{m,e}$, $1/\tau^m_{\mathrm{nr}}$ and $1/\tau_{\mathrm{dis}}^{m,e}$ are carrier capture rate, cascaded relaxation rate into the QD GS, thermal escape rate up into higher energy levels, standard non-radiative recombination rate and dislocation-induced non-radiative recombination rate [28, 29], respectively; N^e_m is the electron number in section $w \times \Delta z$, with m = BL, WL, ES2, ES1, GS.

The rate equation in the QD active region for the GS carrier number in the section $w \times \Delta z$ and the photon density S can be described as:

$$\frac{dN^e_{\mathrm{GS}}}{dt} = \frac{N^e_{\mathrm{ES1}} f^{e\prime}_{\mathrm{GS}}}{\tau^{e}_{0}} - \frac{N^e_{\mathrm{GS}} f^{e\prime}_{\mathrm{ES1}}}{\tau^{\mathrm{GS},e}_{\mathrm{esc}}} - \frac{N^e_{\mathrm{GS}}}{\tau^{\mathrm{GS},e}_{\mathrm{nr}}} - v_{\mathrm{gr}} \frac{g^{\max}_{\mathrm{mat}}\left(f^e_{\mathrm{GS}} + f^h_{\mathrm{QD}} - 1\right)}{1 + \varepsilon S} S \cdot \frac{V_{\mathrm{AR}}\Delta z}{L} \quad (5)$$

with a material gain $g^{\max}_{\mathrm{mat}}$, $f^h_{\mathrm{QD}} = 0.5$ and active region volume V_{AR}. The photon density is calculated by the forward and reverse propagating electric fields E_{F} and E_{R}

$$S = |E_{\mathrm{F}}|^2 + |E_{\mathrm{R}}|^2 \quad (6)$$

where field E_{F} and $E_{\mathrm{R}}$are derived from equation (7) including confinement factor Γ, field gain g, field loss α_i, and field spontaneous noise $i_{\mathrm{F,R}}^{\mathrm{sp}}$ [30].

$$\left(\frac{1}{v_{\mathrm{gr}}}\frac{\partial}{\partial t}\pm\frac{\partial}{\partial z}\right)E_{\mathrm{F,R}}\left(z,t\right)=\left(\Gamma g-\alpha_i\right)E_{\mathrm{F,R}}\left(z,t\right)+i_{\mathrm{F,R}}^{\mathrm{sp}}\left(z,t\right) \quad (7)$$

where $g=\frac{g_{\mathrm{mat}}^{\mathrm{max}}\left(f_{\mathrm{GS}}^{e}+f_{\mathrm{QD}}^{h}-1\right)}{2(1+\varepsilon S)}$,

We can combine the above equations with the assumption that the photon density S is zero, at a steady state of below and near threshold, where the I_{th} is determined by

$$\frac{\eta I_{\mathrm{th}}}{e}\frac{\Delta z}{L}=\frac{N_{\mathrm{BL}}^{e}}{\tau_{\mathrm{nr}}^{\mathrm{BL}}}+\frac{N_{\mathrm{WL}}^{e}}{\tau_{\mathrm{nr}}^{\mathrm{WL}}}+\frac{N_{\mathrm{GS}}^{e}}{\tau_{\mathrm{nr}}^{\mathrm{GS},e}}+\frac{N_{\mathrm{BL}}^{e}}{\tau_{\mathrm{dis}}^{\mathrm{WL},e}}+\frac{N_{\mathrm{WL}}^{e}}{\tau_{\mathrm{dis}}^{\mathrm{BL},e}}+v_{\mathrm{gr}}g_{\mathrm{th}}S\cdot\frac{V_{\mathrm{AR}}\Delta z}{L}. \quad (8)$$

Generally, τ_{dis}^{-1} is considered a major factor for the REDR, and here we assume $R_{\mathrm{dis}}=\tau_{\mathrm{dis}}^{-1}=AN_d\left(t\right)$ accounts for the non-radiative carrier capture rate at the defect site with a defect density $N_d\left(t\right)$ where A is a constant. The threshold gain condition $g\left(n\right)=g\left(n_{\mathrm{th}}\right)=g_{\mathrm{th}}$ is satisfied when a laser begins lasing and comes into the steady state, i.e. we are assuming the carrier density n is pinned at the threshold value n_{th}. Furthermore, R_{dis} increases because of the defect sites acting as the non-radiative recombination enhanced centres. A defect-carrier interaction process has been proposed by Chuang [25, 26, 31], where the defect generation rate has the form:

$$\frac{dN_d\left(t\right)}{dt}=K\left(n\right)N_d\left(t\right) \quad (9)$$

where the coefficient $K\left(n\right)$ depends on the physical processes of TD generation. The electron–hole recombination enhances the TD generation at lasing states, while the $K\left(n\right)$ can be described as:

$$K\left(n\right)=\kappa n\left(t\right)p\left(t\right)=\kappa n^2 \quad (10)$$

where $n=p=n_{\mathrm{th}}$ in the undoped active region and κ is a constant which depends on the temperature T and an activation energy E_{a}

$$\kappa=\kappa_0\exp[-E_{\mathrm{a}}/\left(k_{\mathrm{B}}T\right)] \quad (11)$$

where k_{B} is the Boltzmann's constant.

Chuang's model fits their experiment perfectly, in which the samples are well prepared without dark line and dark spot defects, and the only factor for degradation is the point defect density [26]. The energy released by carrier recombination is the source of the creation or growth of TDs. On the other hand, for non-point defect, the defects interact and share the released energy. TD is a kind of defect that interacts strongly, where each defect competes with another defect at a time. In Lam's defect generation model [32], it is assumed that the creation and growth of a type of defect requires certain types of resources.

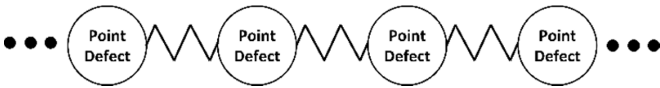

Figure 1. Threading dislocation model.

In our model, TDs are regarded as a line of point defects, which is shown in figure 1. The interaction among point defects is phonon-like and elastic. At the same time, point defects distribute uniformly in an infinite line and every point defect has the same amount of energy because of interactions. If every point defect is dependent with others, then the total energy can be written as:

$$E=\frac{1}{2}k(nx)^2. \quad (12)$$

If every point defect is independent with others, then the total energy can be written as

$$E=n\frac{1}{2}k(x)^2 \quad (13)$$

where k is a constant factor characteristic of the spring, x is the displacement of each point defect and n is the number of point defects in the TDs.

There are $N_d\left(t\right)$ possible point defects sharing the total finite energy. We assume these point defects are not independent totally or not dependent completely and the total energy is proportional to $[N_d\left(t\right)]^2+N_d\left(t\right)$.

The defect generation rate with saturation can be described as:

$$\frac{dN_d\left(t\right)}{dt}=K\left(n\right)N_d\left(t\right)-C\left(n\right)\left[N_d\left(t\right)N_d\left(t\right)+N_d\left(t\right)\right] \quad (14)$$

$$C\left(n\right)=cn\left(t\right)p\left(t\right)=cn^2 \quad (15)$$

$$c=c_0\exp[-E_{\mathrm{a}}/\left(k_{\mathrm{B}}T\right)]. \quad (16)$$

The rate of growth of the point defect density is governed by $K\left(n\right)$, while $C\left(n\right)$ controls the rate of saturation of the defect density. We can obtain the solution to this differential equation

$$N_d\left(t\right)=\frac{M\left(n\right)N_d\left(0\right)}{N_d\left(0\right)+\left[M\left(n\right)-N_d\left(0\right)\right]\exp[-C\left(n\right)M\left(n\right)]} \quad (17)$$

where, $M\left(n\right)=\frac{K(n)-C(n)}{C(n)}$, $N_d\left(0\right)$ is the initial defects density. We assume that point defect growth only occurred because of the TD, and the growth of point defect in the BL $N_{d(\mathrm{BL})}$ does not greatly affect the growth of the other defects in the WL $N_{d(\mathrm{WL})}$. $\Delta I_{\mathrm{th}}\left(t\right)$ can be obtained from (8) as the following solvable for:

$$\Delta I_{\rm th}(t)=\frac{eL}{\eta\Delta z}\left[A_{\rm BL}\left(\frac{{\rm M}_{\rm (BL)}(n)N_{d{\rm (BL)}}(0)}{N_{d{\rm (BL)}}(0)+[{\rm M}_{\rm (BL)}(n)-N_{d{\rm (BL)}}(0)]\exp[-c_{\rm (BL)}(n)M_{\rm (BL)}(n)t]}-N_{d{\rm (BL)}}(0)\right)N^{e}_{\rm BL}+A_{\rm WL}\left(\frac{{\rm M}_{\rm (WL)}(n)N_{d{\rm (WL)}}(0)}{N_{d{\rm (WL)}}(0)+[{\rm M}_{\rm (WL)}(n)-N_{d{\rm (WL)}}(0)]\exp[-c_{\rm (WL)}(n)M_{\rm (WL)}(n)t]}-N_{d{\rm (WL)}}(0)\right)N^{e}_{\rm WL}\right]. \tag{18}$$

To simplify the equation, we assume parameters in BL and WL are the same because the TD and carrier density in BL and WL are nearly identical. We can obtain:

$$\Delta I_{\rm th}(t)=\frac{eV_{\rm WL}An^{e}_{\rm th}}{\eta}\left[\left(\frac{M(n)N(0)}{N_d(0)+[M(n)-N_d(0)]\exp[-C(n)M(n)t]}-N_d(0)\right)\right] \tag{19}$$

where $n^{e}_{\rm th}=N^{e}_{\rm th}/\Delta zwd_{\rm WL}$, and $V_{\rm WL}=Lwd_{\rm WL}$.

3. Results and discussion

Here, we employ the degradation data on the InAs/GaAs QD laser epitaxially grown directly on a Si substrate in [22]. The ageing process was tested at the temperature of 26 °C and the drive current of 210 mA, which equals to 1.75 times the $I_{\rm th}$. The ageing results and fitting curve according to equation (17) curve fitting parameters are shown in figure 2 and in table 1, respectively. Most of the increase in the $I_{\rm th}$ occurred in the early stage of testing, and then followed by a very slow change. The fitting curve fits the data well in the early stage, while the deviation occurs and become serious in the longer stages. The internal optical loss is a major factor that causes the increase in threshold current density ($J_{\rm th}$) during the initial degradation. The fitting curve of internal optical loss due to the presence of TDs is shown in figure 3, from which we can see the measured internal optical loss matches the fitting curve quite well. Therefore, we can deduce that the TDs play a major role in the $I_{\rm th}$ increase in the early stage that affect the $I_{\rm th}$ increase can be negligible in the initial ageing stage.

The light output against current (*L–I*) characteristics of QD laser are modelled using rate equations as a function of the laser cavity length of 3 mm, 3.2 mm and 4 mm, respectively as shown in figure 4(a). The QD parameters referring to the article [23] are listed in table 2, and the TDD is chosen to $6\times10^{6}\,{\rm cm}^{-2}$. It apparently shows that the $J_{\rm th}$ of long cavity is lower than the short one. For QD laser directly grown on Si substrates, TD is the main factor that causes the degradation in the early stage, and this kind of defects largely exists in the WL of QDs. We simulate the carrier density in WL using travelling wave rate equations under various current density conditions, which is shown in figure 4(b). Here, we assume that all parameters are the same for lasers with laser length is between 3 mm and 4 mm except $J_{\rm th}$. The current density of the WL should be pinned at a constant, however, the simulation results show that the current density of the WL varies with the input current. Therefore, when the input current density is above $J_{\rm th}$, the increasing input current leads to an increasing rate of degradation. However, the current density variation is relatively small and its effect on the rate of degradation is insignificant. Using fitted coefficient and simulating carrier density, where the input current of the laser of length of 3.2 mm is chosen to be 1.7 times of $I_{\rm th}$ and the other input currents are chosen to be 1.3 times of $I_{\rm th}$, the rates of degradation or the $J_{\rm th}$ variations of various laser lengths are calculated using parameters in table 1 and drawn in figure 4(c). It manifests that the increase of $J_{\rm th}$ of shorter laser is more rapid than that of longer one, which corresponds to the same result in paper from [24].

For QW laser, a two-level system with BL and QWs is used to simulate the lasing action. Rate equations similar to those used for the QD laser model are modified to be applied in QWs laser.

$$\frac{dN^{e,h}_{\rm BL}}{dt}=\frac{\eta I}{e}\frac{\Delta z}{L}+\frac{N^{e,h}_{\rm QW}f^{e,h'}_{\rm BL}}{\tau^{{\rm QW},e,h}_{\rm esc}}-\frac{N^{e,h}_{\rm BL}f^{e,h'}_{\rm QW}}{\tau^{{\rm QW},e,h}_{c}}-\frac{N^{e,h}_{\rm BL}}{\tau^{\rm BL}_{\rm nr}}-\frac{N^{e,h}_{\rm BL}}{\tau^{{\rm BL},e,h}_{\rm dis}} \tag{20}$$

$$\frac{dN^{e,h}_{\rm QW}}{dt}=\frac{N^{e,h}_{\rm BL}f^{e,h'}_{\rm QW}}{\tau^{{\rm QW},e,h}_{c}}-\frac{N^{e,h}_{\rm QW}f^{e,h'}_{\rm BL}}{\tau^{{\rm QW},e,h}_{\rm esc}}-\frac{N^{e,h}_{\rm QW}}{\tau^{\rm QW}_{\rm nr}}-\frac{N^{e,h}_{\rm QW}}{\tau^{{\rm QW},e,h}_{\rm dis}}-v_{\rm gr}g_0\ln\left(\frac{n^{e}_{\rm QW}}{n_0}\right)S\cdot\frac{V_{\rm AR}\Delta z}{L} \tag{21}$$

where $n^{e}_{\rm QW}$ is the QW electron density and n_0 is the transparency carrier density. The *L–I* characteristics of QW lasers with a dislocation density of 6×10^{6} cm^{-2} are shown in figure 5(a), and corresponding parameters are listed in table 2. Carrier density versus input current density simulation of the QW laser is shown in figure 5(b), the current is pinned at the $I_{\rm th}$. The

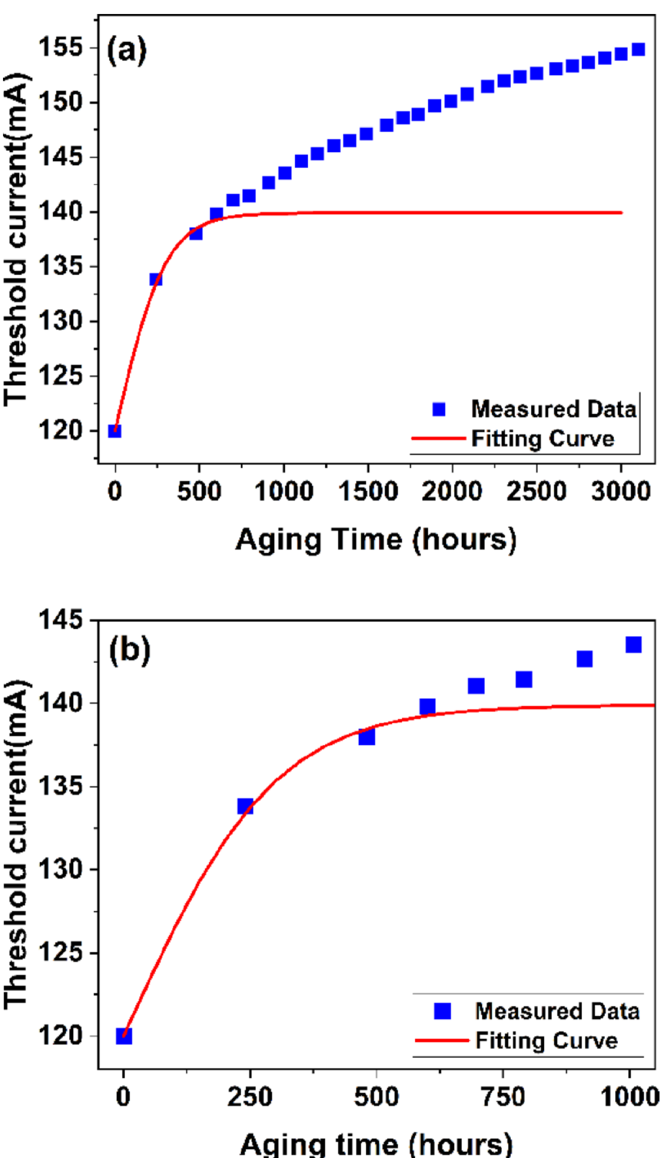

Figure 2. (a) I_{th} versus continuous-wave (CW) operating time for lasers with cavity length of 3.2 mm, at 26 °C and fitting I_{th}. (b) Zoomed (a).

Table 1. Fitted coefficient (3.2 mm QD) and calculated coefficient (others)

	3.2 mm QD	3 mm QD	4 mm QD	3 mm QW
I_{th0} (mA)	120	116.5	130	12 000
Scaled $eV_{WL}An^{e}_{th}/\eta$ (mA cm^3)	0.662	0.696	0.527	202.3
Scaled $cn^2_{th}\exp - (E_a/kT)$ (10^{-4} cm^3 h^{-1})	1.19	1.317	0.7554	11.12×10^4
Scaled M (cm^{-3})	58.07	58.07	58.07	58.07
Scaled $N_d(0)$ (cm^{-3})	28	28	28	28
Simulated n^e_{th} (cm^{-3})	6.158×10^{15}	6.47×10^{15}	4.896×10^{15}	1.89×10^{18}

threshold carrier density n^e_{th} of the QW laser is several orders of magnitude larger than that of the QD lasers. The degradation in the early stage is calculated using fitting parameters A and c that are assumed to be the same as the QD laser. The rate of degradation of the QW laser is calculated using parameters in table 1 and shown in figure 5(c), and it is manifest that the degradation of the QW laser is more rapid than the degradation of QD lasers with the same dislocation density in the early stage of ageing.

To further investigate the impact of TDs to the lasers for real application in data transmission, the small signal response [33] of the aged QD laser based on the rate equation model has been calculated. The results are shown in figure 6. We assume the I_{th} varies with the ageing time, and the only reason

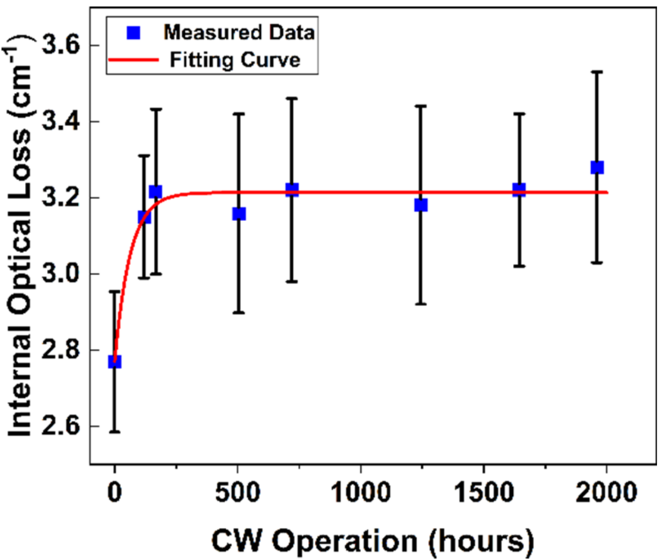

Figure 3. Internal optical loss versus CW operating time.

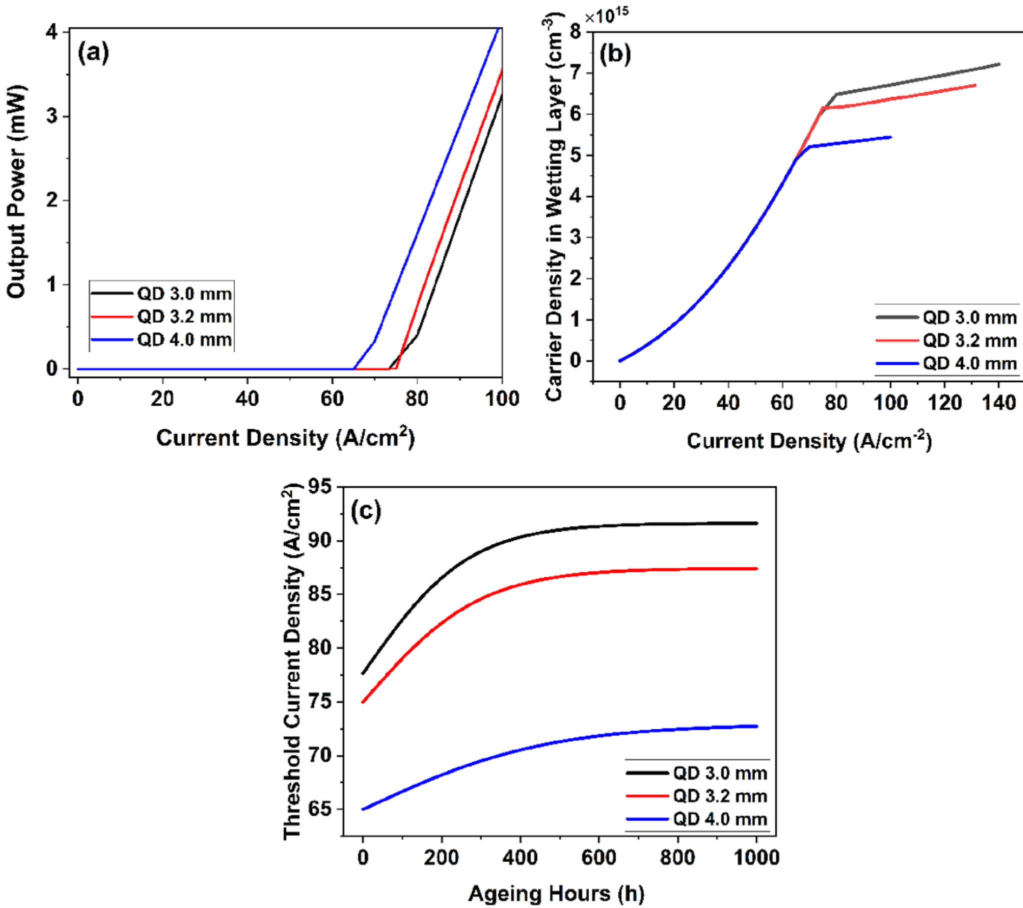

Figure 4. (a) *L–I* characteristic simulations of QD lasers of different length before the ageing test. (b) Carrier density in WL versus input current density simulations of QD lasers of different length. (c) Rate of degradation simulations of QD lasers of different lengths.

for the variation is the TD defect growth. The corresponding 3 dB bandwidth decreases with the defect growth. The 3 dB bandwidth of the QD laser with a current of 200 mA, is 1.5 GHz for the laser of I_{th} of 120 mA and decreases to 1.47 GHz and 1.34 GHz with an increasing I_{th} of 130 mA and 140 mA, respectively. On the other hand, the 3 dB bandwidth of the QD laser increases as one would expect as the drive current is increased more. The 3 dB bandwidth is increased

Table 2. Parameter used for QW and QD simulation.

QD parameters	QW parameters	Parameters unchanged for QD and QW simulations:
Laser wavelength $\lambda_{QD} = 1310$ nm Modal gain $g_{mod} = 25$ cm^{-1} Optical confinement factor $\Gamma = 0.005$ Gain saturation factor $\varepsilon = 5 \times 10^{16}$ cm^3 QD degeneracies $p_i = 2, 4, 6, 6,$ 6 (GS, ES1–ES4) QD carrier capture time $\tau_c^{QD,e,h} = 3$ ps, 0.5 ps Intradot relaxation time $\tau_0^e = 250$ fs QD density $\rho = 4 \times 10^{10}$ cm^{-2}	Laser wavelength $\lambda_{QW} = 980$ nm Gain constant $g_0 = 3000$ cm^{-1} Optical confinement factor $\Gamma = 0.02$ Gain saturation factor $\varepsilon = 1 \times 10^{17}$ cm^3 Transparency current density $n_0 = 1.6 \times 10^{18}$ cm^{-3}	Laser length $L = 3$ mm Waveguide width $w = 50$ μm Facet reflectivity $R_1 = R_2 = 0.3$ Number of active layers $N_{layers} = 5$ Diffusion constant $D_{GaAs}^{e,h} = 191$ cm^2 s^{-1}, 10 cm^2 s^{-1} Group velocity $v_{gr} = 8.4 \times 10^7$ m s^{-1} Active region volume $V_{AR} = 6 \times 10^{-9}$ cm^3 BL thickness $h_{BL} = 40$ nm WL/QW thickness: $h_{WL,QW} = 8$ nm Diffusion constant $D_{InGaAs}^{e,h} = 176$ cm^2 s^{-1}, 8 cm^2 s^{-1} Current injection efficiency $\eta = 0.55$ WL/QW transport/capture time $\tau_c^{WL,e,h} = 6.4$ ps, 8.2 ps BL, WL/QW, and QD carrier lifetime $\tau_{nr}^{e,h} = 2.8$ ns Waveguide loss $\alpha_i = 3$ cm^{-1}

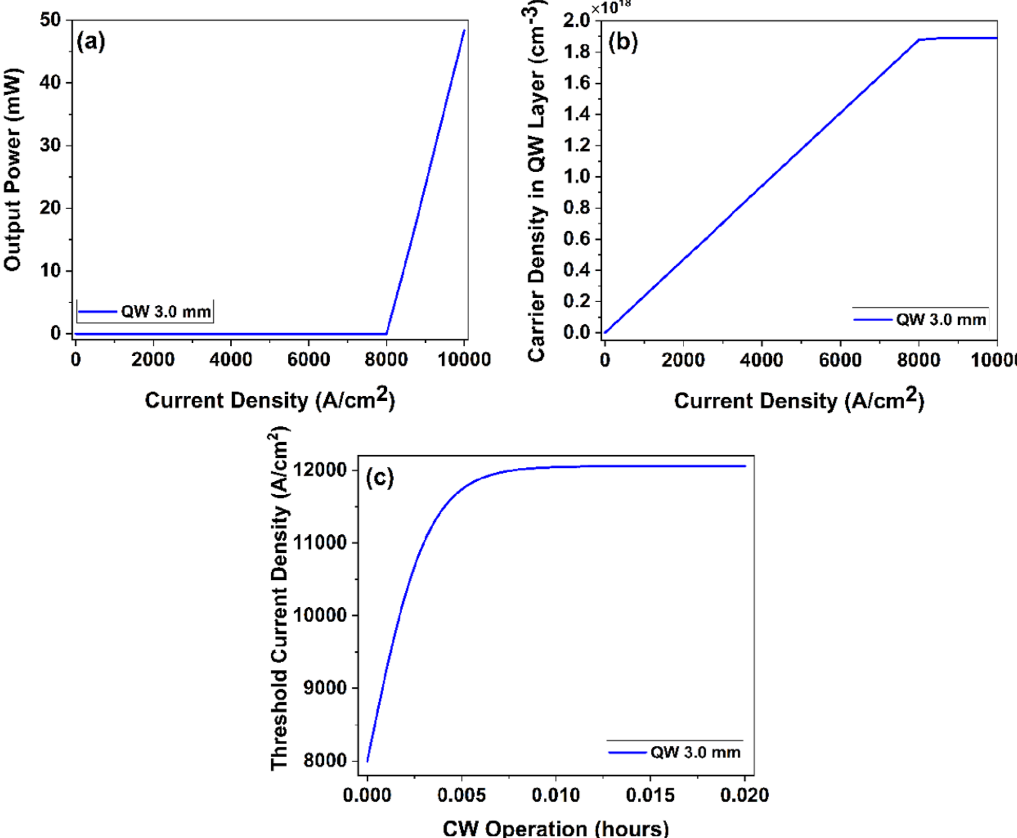

Figure 5. (a) *L–I* characteristic simulation of QW lasers of the length of 3 mm. (b) Carrier density of QW versus input current density simulation of QW lasers of the length of 3 mm. (c) Rate of degradation simulation of QW lasers of the length of 3 mm.

from 1.5 GHz to 1.63 GHz and 1.76 GHz due to the current raised from 200 mA to 220 mA and 240 mA, respectively. The 3 dB line width versus the square root of current minus threshold current (figure 6(b)) is plotted. The proportional constant (modulation current efficiency) [34] is about 0.12 GHz/mA0.5, and the proportional constant nearly does

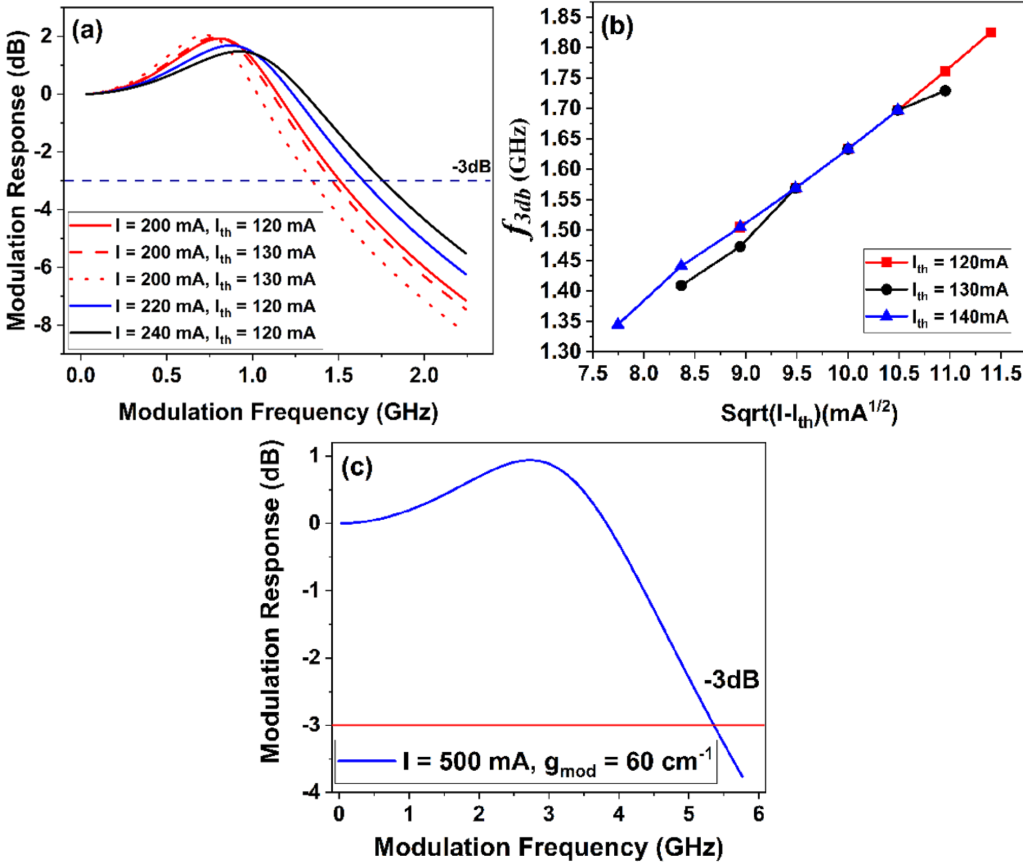

Figure 6. (a) Small-signal modulation response curves of a 3.2 mm length QD laser on Si length with I_{th} of 120, 130, and 140 mA recorded at 200 mA, and I_{th} of 120 mA at current of 220 mA and 240 mA. (b) 3 dB line width as a function of the square root current above threshold $(I–I_{th})^{1/2}$, the modulation efficiency is nearly a constant. (c) Higher 3 dB line width by increasing the modal gain and the current.

not vary with the ageing of the laser. The major factor of the 3 dB bandwidth is the gain, and the 3 dB bandwidth of the QD laser including up to ten QD layers or more for high gain of 60 cm^{-1} with current of 500 mA is calculated, which illustrates that the 3 dB bandwidth can be up to 5.35 GHz by increasing the modal gain and the current.

4. Conclusion

We have presented a theoretical study on the degradation of QD laser monolithically grown on Si substrate with enhanced non-radiative recombination because of the TDs and compared the impacts of TDs on QD and QW lasers. An analytical ageing expression including the saturation term caused by interaction of the defect type of TDs was derived. Our phenomenological model successfully reproduces the trends of degradation because of TDs, which is consistent with internal optical loss of the laser due to an increased presence of defects. The threshold carrier density and TDD in WL or BL are the main factors to determine the ageing speed, as we compared J_{th} threshold current density, carrier density and degradation of different length laser. The comparison reveals the longer the laser cavity, the lower the rate of degradation, which is attributed to the lower the J_{th}. Ignoring the effects of other defect reactions except TD-induced reactions, our simulations show that QW lasers are more severely affected than QD lasers. The study presented here is the first theoretical approach to assessing the rate of degradation caused by TDs for QD and QW laser in the early operation stage and hence further enhances the understanding of performance of QD lasers as the lasers age in the stage that the internal optical loss increases significantly. The comparison of small signal response of the aged QD laser was discussed, the corresponding 3 dB bandwidth decreases with the defect growth. To realise the experiment as future work, laser device lifetime measurement based on the different laser cavity length will be carried out. The certain TDD value can be obtained by growing different types and thickness of III–V buffer layers, with high-temperature thermal cycle annealing process [35].

Data availability statement

The data that support the findings of this study are available upon reasonable request from the authors.

Funding

This work was supported in part by YIPA, CAS (2019226), UK Engineering and Physical Sciences Research Council (EP/P006973/1, EP/T01394X/1, EP/T028475/1 and

National Epitaxy Facility), European project H2020-ICT-PICTURE (780930) and Royal Academy of Engineering (RF201617/16/28). National Key Research and Development Program of China (2021YEB2800500), NSFC (61574138, 61974131), NSF of Zhejiang Province (LGJ21F050001), and Major Scientific Research Project of Zhejiang Lab (2019MB0AD01). Jianzhuo Liu thanks CAS Scholarship.

ORCID iDs

Mingchu Tang https://orcid.org/0000-0001-6626-3389
Siming Chen https://orcid.org/0000-0002-4361-0664
Huiyun Liu https://orcid.org/0000-0002-7654-8553

References

[1] Helkey R, Saleh A, Buckwalter J and Bowers J 2019 *IEEE J. Sel. Top. Quantum Electron.* **25** 1
[2] Sabella R 2019 *IEEE J. Sel. Top. Quantum Electron.* **26** 8301611
[3] Wan Y *et al* 2021 *Laser Photon. Rev.* **15** 2100057
[4] Wan Y *et al* 2020 *Laser Photon. Rev.* **14** 1900348
[5] Mikulics M and Hardtdegen H 2020 *FlatChem* **23** 100186
[6] Wan Y *et al* 2020 *Laser Photon. Rev.* **14** 2000037
[7] Chow W, Wan Y, Bowers J and Grillot F 2022 *Laser Photon. Rev.* **16** 2100620
[8] Cuyvers S *et al* 2021 *Laser Photon. Rev.* **15** 2000485
[9] Pan S, Cao V, Liao M, Lu Y, Liu Z, Tang M, Chen S, Seeds A and Liu H 2019 *J. Semiconduct.* **40** 101302
[10] Tang M, Park J-S, Wang Z, Chen S, Jurczak P, Seeds A and Liu H 2019 *Prog. Quantum Electron.* **66** 1–18
[11] Tang M, Chen S, Wu J, Jiang Q, Dorogan V, Benamara M, Mazur Y, Salamo G, Seeds A and Liu H 2014 *Opt. Express* **22** 11528–35
[12] Liu A, Herrick R, Ueda O, Petroff P, Gossard A and Bowers J 2015 *IEEE J. Sel. Top. Quantum Electron.* **21** 1
[13] Liang H, Jin T, Chi C, Sun J, Zhang X, You T, Zhou M, Lin J and Wang S 2021 *Opt. Express* **29** 38465–76
[14] Wang J, Hu H, Yin H, Bai Y, Li J, Wei X, Liu Y, Huang Y, Ren X and Liu H 2018 *Photon. Res.* **6** 321–5
[15] Chen S, Liao M, Tang M, Wu J, Martin M, Baron T, Seeds A and Liu H 2017 *Opt. Express* **25** 4632–9
[16] Jung D *et al* 2018 *ACS Photonics* **5** 1094–100
[17] Mikulics M, Mayer J and Hardtdegen H 2022 *J. Appl. Phys.* **131** 110903
[18] Peng Y, Mou Y, Wang T, Wang H, Liang R, Wang X, Chen M and Luo X 2019 *IEEE Trans. Electron Devices* **66** 2637–42
[19] Mikulics M, Kordoš P, Fox A, Kočan M, Lüth H, Sofer Z and Hardtdegen H 2017 *Appl. Mater. Today* **7** 134–7
[20] Mehmet A, Charles A, Stanton E and James P 2004 *3rd Int. Conf. on Solid State Lighting Proc SPIE* p 5187
[21] Kazi Z, Thilakan P, Egawa T, Umeno M and Jimbo T 2001 *Jpn. J. Appl. Phys.* **40** 4903
[22] Chen S *et al* 2016 *Nat. Photon.* **10** 307–11
[23] Liu Z *et al* 2020 *J. Lightwave Technol.* **38** 240–8
[24] Shutts S, Allford C, Spinnler C, Li Z, Sobiesierski A, Tang M, Liu H and Smowton P 2019 *IEEE J. Sel. Top. Quantum Electron.* **25** 1
[25] Chuang S, Ishibashi A, Kijima S, Nakayama N, Ukita M and Taniguchi S 1997 *IEEE J. Quantum Electron.* **33** 970–9
[26] Chuang S, Nakayama N, Ishibashi A, Taniguchi S and Nakano K 1998 *IEEE J. Quantum Electron.* **34** 851–7
[27] Sim S 1990 A review of the reliability of III–V opto-electronic components *Semiconductor Device Reliability* vol 175, ed A Christou and B A Unger (Dordrecht: Springer) p 301
[28] Hantschmann C, Liu Z, Tang M, Seeds A, Liu H, White I and Richard P 2020 *Proc. SPIE* **11274** 112740J
[29] Chernyak L, Osinsky A and Schulte A 2001 *Solid-State Electron.* **45** 1687–702
[30] Hantschmann C, Vasil'ev P, Chen S, Liao M, Seeds A, Liu H, Penty R and White I 2018 *J. Lightwave Technol.* **36** 3837–42
[31] Chuang S 1996 *Appl. Phys. Lett.* **69** 1588
[32] Lam S K K, Mallard R E and Cassidy D T 2003 *J. Appl. Phys.* **94** 1803
[33] Wang L, Wang Y, Francis H, Lu R, Xia M, Liu F, Hopkinson M and Jin C 2020 *Opt. Express* **28** 16486–96
[34] Hantschmann C, Vasil'ev P, Chen S, Liao M, Seeds A, Liu H, Penty R and White I 2018 *European Conf. on Optical Communication (ECOC)* (*Rome*) p 1
[35] Shang C, Selvidge J, Hughes E, Norman J C, Taylor A A, Gossard A C, Mukherjee K and Bowers J E 2021 *Phys. Status Solidi* a **218** 2000402